Journal of Materials Chemistry A

COMMUNICATION

View Article Online
View Journal

Cite this: DOI: 10.1039/c5ta10639g

Received 25th December 2015
Accepted 11th January 2016

DOI: 10.1039/c5ta10639g

www.rsc.org/MaterialsA

Three-dimensional interconnected Ni_{core}–NiO_{shell} nanowire networks for lithium microbattery architectures†

Alexandru Vlad,*[a] Vlad-Andrei Antohe,[a] Juan Manuel Martinez-Huerta,[a] Etienne Ferain,[b] Jean-François Gohy[a] and Luc Piraux*[a]

We report a simple and reliable route for the synthesis of three-dimensional bicontinuous Ni–NiO core–shell nanowire networks. The interconnected architecture is self-supported and provides rapid ion and charge collection pathways, as well as efficiently accommodates the volume change induced stress resulting in enhanced lithium storage properties. The capacity per footprint area is 40 times higher than that of a 2D system at an equivalent active material thickness.

Three-dimensional (3D) nanowire networks (NWNs) are expected to play an important role in the development of the next generation of nano-devices as the high degree of wire interconnectivity could be beneficial to a wide range of applications including energy storage,[1–4] sensors,[5] catalysts,[6] electrochromic devices,[7] magnetic devices[8] and solar cells,[9] among others.

For microbattery applications in particular, electrodes made of 3D-NWNs are very appealing since they combine the benefits of nanoconfinement such as short diffusion pathways, rapid charge collection and facile accommodation of mechanical constraints, with high areal active electrode material mass loading[10,11] and structural stability. Such developments have become particularly interesting in the context of 3D microbattery manufacturing where electrode configurations that provide high power while maintaining high specific footprint capacities are critical.[12,13] Many structures have been proposed in the past, with nanowire, nanotubular or core–shell architectures being the most promising.[14–19]

However, the fabrication of 3D-NWN-based microbattery electrodes with a regular long-range order arrangement through simple processes remains challenging to date. Several strategies have been proposed over the past for the fabrication of ordered 3D-NWNs, including chemical self-assembly growth methods.[20,21] The template approach remains however the most promising route for reliable synthesis of periodic 3D NW-like networks with a controlled morphology. Such 3D NWNs are obtained through a growth mechanism involving electrochemical processes or sol–gel reactions using hierarchical pore structures as a template. A large variety of templates have been used for this purpose including silica templates,[22] track-etched polymer membranes,[6,8] diblock copolymers[7] and 3D alumina templates.[3,23] However, the added value of such configuration on the electrochemical performances for battery applications has been poorly explored.[2–7,13,14]

In the present work, we detail on a versatile bottom-up strategy for the growth of free-standing arrays of 3D interconnected core–shell metal–metal oxide NWNs with potential for microbattery applications. Ni and NiO are selected as an example of low-cost semiconductor and naturally abundant materials. The method involves Ni plating within 3D ordered nanoporous track-etched polymer membranes with crossed cylindrical nanopores followed by controlled thermal conversion[24,25] of Ni into interconnected Ni–NiO core–shell nanowires (Ni_{core}–NiO_{shell}). The designed 3D Ni_{core}–NiO_{shell} NWN tested as a microbattery electrode material shows clear advantages in terms of cycling stability, rate capability and attainable specific area capacities over the 2D thin-film or 3D macroporous electrodes with a similar composition.

Results and discussion

The interconnected nanoporous templates have been prepared by performing a sequential two-step exposure to energetic heavy ions, at angles of +25° and −25° with respect to the normal of the polycarbonate (PC) membrane surface.[8] The experimental details are provided in the ESI.† Fig. 1a briefly outlines the fabrication process whereas Fig. 1b displays the morphology of the Ni 3D-NWN obtained after plating and template dissolution.

The 3D-NWNs are characterized by dense arrays of interconnected cylindrical NWs, being the inverse replica of the nanoporous polymer template. The NWNs also show

[a]Institute of Condensed Matter and Nanosciences, Université Catholique de Louvain, Place Croix du Sud 1 and Place L. Pasteur 1, B-1348, Louvain-la-Neuve, Belgium. E-mail: alexandru.vlad@uclouvain.be; luc.piraux@uclouvain.be

[b]it4ip s.a., Avenue Jean-Etienne Lenoir, B-1348 Louvain-la-Neuve, Belgium

† Electronic supplementary information (ESI) available: Fabrication and electrochemical characterization details. See DOI: 10.1039/c5ta10639g

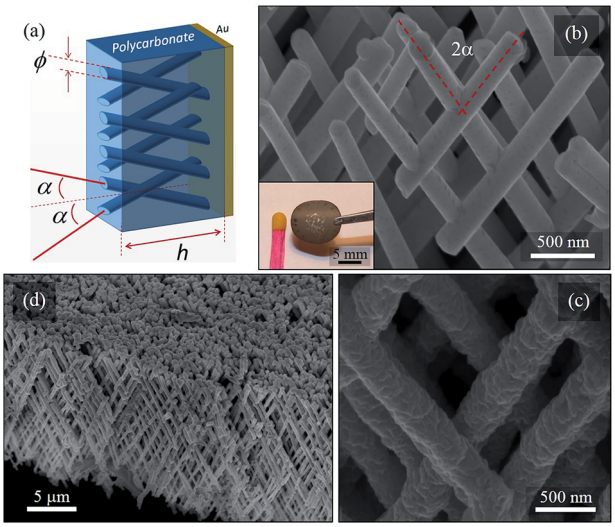

Fig. 1 (a) Schematic representation of a PC membrane with crossed cylindrical nanopores oriented at angles $\alpha = \pm 25°$ normal to the PC surface. (b) SEM micrograph of the interconnected array of electrodeposited 3D Ni NWNs with an inset optical image showing the mechanical robustness of the macroscopic self-supporting network. The average intersection angle between crossed NWs was estimated to be $2\alpha \cong 50°$. (c) SEM micrograph of the 3D Ni_{core}–NiO_{shell} NWN obtained by oxidation in air at 450 °C for 60 min. (d) Low-magnification tilted view of the dense interconnected 3D Ni_{core}–NiO_{shell} NWs.

homogeneous unions at the vertices, which form an angle of $2\alpha = 50°$ along the out-of-plane direction. The as-prepared Ni 3D-NWNs are self-supported and can be manipulated easily without noticeable mechanical damage, as highlighted in the inset in Fig. 1b.

The electrode active material was grown onto the Ni 3D-NWN *via* simple annealing in air, by progressively converting Ni into NiO.[24,25] The conversion of the metallic Ni NWs into Ni_{core}–NiO_{shell} NWs increases the wire diameter and surface roughness (Fig. 1c and d). After annealing at 450 °C for 60 min, the NW average diameter was increased from 230 nm to a mean value of about 305 nm. To confirm the partial oxidation of the Ni nanowires as well as the formation of the NiO phase, composition mapping (EDX), X-ray diffraction (XRD) and magnetization analyses were carried out. The EDX spectra of the interconnected 3D-NWN before and after 60 minutes annealing in air at 450 °C are shown in Fig. 2a and b, respectively. Semi-quantitative compositional and elemental analysis of the annealed sample is also reported in the inset of Fig. 2b, corroborating partial oxidation of the Ni NWs. Fig. 2c shows the XRD pattern of the interconnected 3D Ni_{core}–NiO_{shell} NWN. The main diffraction peaks corresponding to the (111), (200) and (220) Miller indices of Ni and NiO suggest as well partial oxidation of the metallic NWs.

Fig. 2d shows the effect of the annealing on the magnetic hysteresis loop of the Ni NWN. The data obtained at room temperature with the magnetic field applied in the out-of-plane direction were normalized to the measured saturation magnetization for the non-annealed reference sample. For all samples, the magnetization was saturated at 2 kOe. In comparison to pristine, non-oxidized samples, the annealed samples show

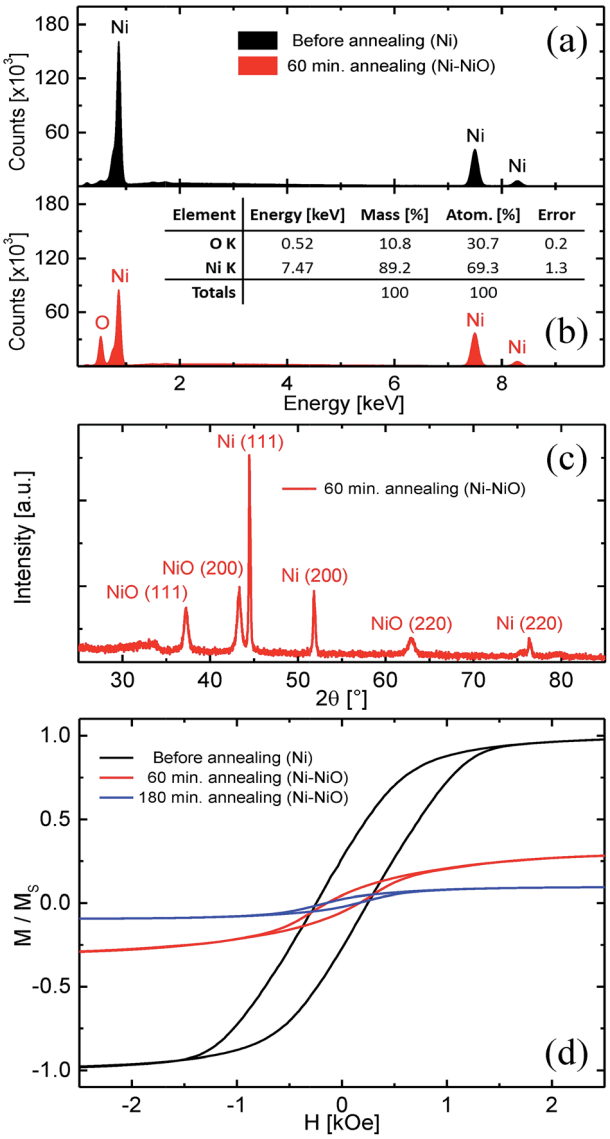

Fig. 2 EDX spectra acquired on the (a) 3D Ni NWN and (b) 3D Ni_{core}–NiO_{shell} NWN. Inset in (b) quantitative compositional analysis of the 3D Ni_{core}–NiO_{shell} NWN. (c) XRD pattern of the 3D Ni_{core}–NiO_{shell} NWN. (d) Magnetization hysteresis loops with the magnetic field perpendicularly applied to the sample surface. The data are normalized with respect to the measured magnetization saturation for the non-annealed sample.

a significant decrease of the saturation magnetic moment, to about 33% and 10% of the initial value for the annealing duration of 60 and 180 minutes, respectively. This further supports the progressive oxidation of the Ni NWs leading to the formation of 3D Ni_{core}–NiO_{shell} NWNs.

Based on the magnetisation response, as the annealing time of Ni NWs was increased, the resulting metallic Ni core decreased gradually, thus leading to a smaller saturation magnetic moment. At the saturation field of 2 kOe, the antiferromagnetic signal from the NiO shell is many orders of magnitude smaller than that due to the ferromagnetic core material and thus it can be neglected. Under this assumption,

the diameter of the Ni core is estimated to be about 135 nm for the sample annealed for 60 min. The estimated volume percentage of Ni is 20%, corresponding to a content of about 25 wt% for the metallic Ni core, closely corroborating the estimations from the EDX and XRD analysis detailed above. Furthermore, an easy estimation shows that Ni_{core}–NiO_{shell} NWs with a Ni core diameter of 135 nm and NiO shell thickness of 85 nm should lead to a mass percentage of oxygen of 12.5%, close to that obtained from the EDX analysis (10.8%, see the inset of Fig. 2b). The observed magnetic behaviour further supported by EDX and XRD analysis confirms the proposed scenario for progressive growth of the NiO_{shell} around the Ni_{core} during the annealing. Fully oxidized Ni 3D-NWNs were obtained by annealing the 230 nm nanowires for more than 4 hours.

Next, the electrochemical characterization of the 3D Ni_{core}–NiO_{shell} NWN microelectrodes was performed. Galvanostatic charge–discharge cycling results are shown in Fig. 3a. The Ni_{core}–NiO_{shell} 3D-NWN electrode shows stable cycling with minimal degradation and good power-rate performances. In turn, the NiO 3D-NWN electrode (obtained by fully oxidizing the 3D Ni NWNs) displays more pronounced capacity degradation, and power-rate limitations.

The superior performances of the Ni_{core}–NiO_{shell} 3D-NWN electrode are the result of the particular architecture where the nanoscale NiO_{shell} layer grown on the Ni_{core} configuration allows for efficient charge collection and ion diffusion (see Fig. S1† and related discussion). This is also visible in the charge–discharge plots of the Ni_{core}–NiO_{shell} 3D-NWN electrode where little polarization is observed when the cycling rate increases from C/10 to 1C (Fig. 3b). Ni_{core} can also ensure structural stability during lithiation-induced volume changes of NiO_{shell} explaining the improved cycling stability. Noticeably, Ni_{core}–NiO_{shell} 3D-NWNs also show 25% lower first cycle irreversible capacity loss (Fig. 3a) which could be also assigned to robust behaviour during the lithiation process.

To further highlight the advantages of the interconnected nanowire configuration, we have analysed the electrochemical behaviour of other representative microbattery electrode configurations as schematically depicted in Fig. 3d. In short, NiO was thermally grown on Ni foil, marked as 2D, and Ni foams, marked as macro 3D, given that the characteristic dimensions of the scaffold are in the few-microns range as compared to 3D-NWNs where the structural features range from few tens up to hundreds of nanometers (see the ESI for experimental details and characterisation). Samples denoted with "Thin-Film" were annealed for 60 minutes, similarly to Ni_{core}–NiO_{shell} 3D-NWNs samples, to attain a comparable NiO active material thickness. Samples denoted with "Thick-Film" were annealed for 16 hours, to grow higher amounts of NiO and thus, attain higher capacity per footprint area.

The electrochemical cycling results are shown in Fig. 3d. First, we can notice that the measured capacities per footprint

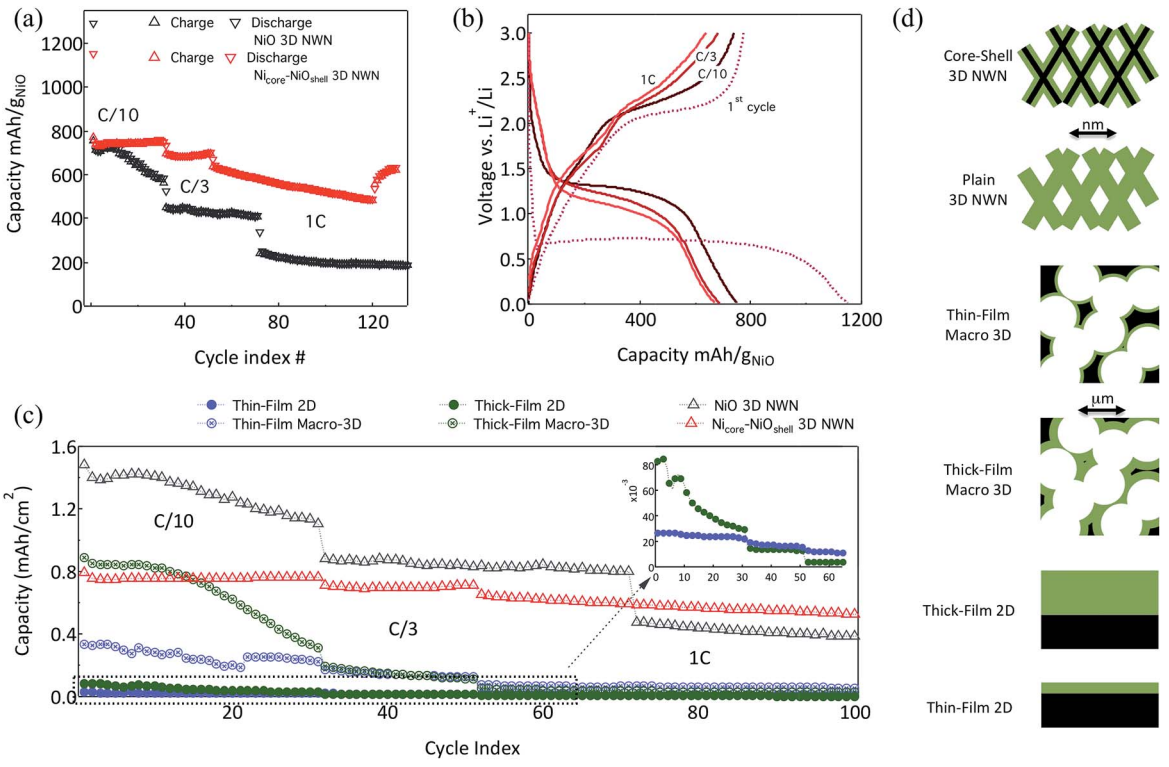

Fig. 3 (a) Cycling behavior at different rates for NiO and Ni_{core}–NiO_{shell} 3D-NWN electrodes. (b) Charge–discharge voltage profiles of the Ni_{core}–NiO_{shell} 3D-NWN electrode for different cycling rates. The first cycle is also shown. (c) Cycling stability plots of the series of 2D and 3D micro- and nano-electrode configurations. (d) Schematic representation of the tested electrodes shown in (c). The gravimetric capacity was calculated with respect to the mass of the NiO contained, with 1C rate corresponding to 765 mA g^{-1} of NiO.

area are consistent with the increased active material film thickness. The cycling stability however is lower for the respective thick-film configuration. Similarly, higher footprint capacities in the series 2D–3D–3D-NWN are measured, consistent with the progressively increased active area in the respective structures. Markedly, amongst all electrode configurations relevant for microbattery applications,[26,27] the Ni_{core}–NiO_{shell} 3D-NWN architecture provides the best cycling stability and power performances with, at the same time, high capacity per footprint area.

To highlight, the electrochemistry of the thin-film 2D and macro-3D configurations is similar to that of the Ni_{core}–NiO_{shell} 3D NWN architecture. This is explained by the fact that NiO films with a comparable thickness were grown on all these samples (see the ESI for experimental and characterization details). However, the capacity per footprint area is 40 times higher than that of thin-film 2D. This is consistent with the estimation presented above, showing that the surface area of the analysed 3D NWN samples is about 50 times higher than their footprint area (or of an equivalent 2D film area).

The NiO 3D-NWN electrode encloses higher energy storage capacity per footprint area (of up to 1.35 mA h cm^{-2}) than the Ni_{core}–NiO_{shell} NWN electrodes as the entire Ni amount is converted to electrochemically active NiO. Similar capacities can be obtained with a thick film configuration; for instance, the thick-film macro-3D configuration has a footprint capacity of 0.8 mA h cm^{-2}. The stability and power performances are in turn negatively affected.

Finally, to confirm the structural robustness of the Ni_{core}–NiO_{shell} 3D NWNs upon cycling, the electrodes were inspected in SEM after 130 lithiation–delithiation cycles. Fig. 4a–c show that the original scaffold morphology is preserved at macro- and micro-scales, with continuous and interconnected NWs spanning the entire electrode thickness surface solid electrolyte interphase accumulation is observed and could account for the observed degradation during cycling. At higher magnifications, the continuous Ni-core could be also visualized (Fig. 4c) further supporting that such structures maintain structural stability upon extended cycling.

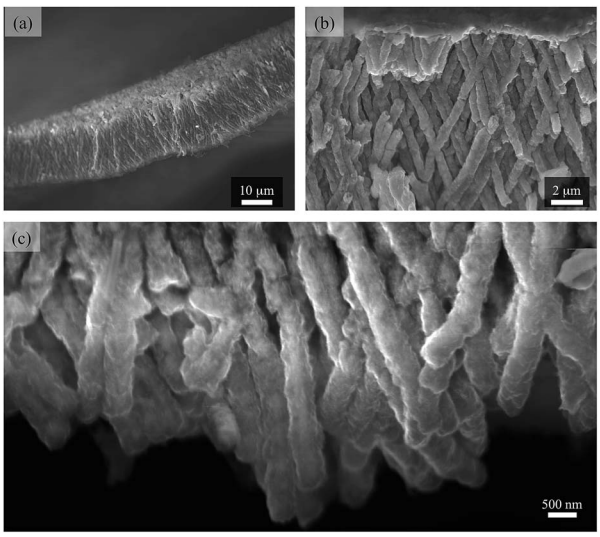

Fig. 4 Post-cycling morphology analysis of the Ni_{core}–NiO_{shell} 3D-NWN electrode. (a and b) Low and high magnification SEM images highlighting that the robust structure is preserved after more than 100 lithiation–delithiation cycles. (c) Zoomed view of interconnected nanowires evidencing limited morphological damage.

Conclusions

This work paves the way for a cost-effective and technically reliable method for building 3D nanostructured electrodes for microbattery applications. The Ni_{core}–NiO_{shell} 3D-NWN microbattery electrode configuration is shown to provide the best performance in terms of footprint capacity, cycling stability and power performances. The enhanced electrochemical performances are assigned to the particular architecture of the nanoelectrodes where the interconnected Ni core ensures mechanical robustness, supports the volume change and warrants efficient charge collection during the lithiation of the redox-active NiO shell. Such architectures can enable orders of magnitude footprint capacity increase while maintaining nanoelectrode characteristic features for rapid ion diffusion and charge collection. Integration of such protocols with microfabrication techniques[12,28] could lead to the development of next generation high power and energy microbatteries.

Acknowledgements

This work was partly supported by the Fédération Wallonie-Bruxelles (ARC 13/18-052 Supracryst). AV and JFG are grateful to the Walloon Region for financial support in the frame of the BATWAL "Programme d'Excellence" and "ERable" Programme.

Notes and references

1 A. Vlad, *et al.*, *Adv. Energy Mater.*, 2015, **5**, 1402115.
2 M. Tian, *et al.*, *J. Power Sources*, 2012, **211**, 46.
3 W. Wang, *et al.*, *Nano Lett.*, 2012, **12**, 655.
4 R. Liu, *et al.*, *Chem. Commun.*, 2011, **47**, 1384.
5 O. S. Kwon, *et al.*, *Chem. Commun.*, 2012, **48**, 10526.
6 M. Rauber, *et al.*, *Nano Lett.*, 2011, **11**, 2304.
7 M. R. J. Scherer and U. Steiner, *Nano Lett.*, 2013, **13**, 3005.
8 E. Araujo, *et al.*, *Nanoscale*, 2015, **7**, 1485.
9 E. J. W. Crossland, *et al.*, *Nano Lett.*, 2009, **9**, 2807.
10 J. Long, *et al.*, *Chem. Rev.*, 2004, **104**, 4463.
11 M. Roberts, *et al.*, *J. Mater. Chem.*, 2011, **21**, 9876.
12 J. H. Pikul, *et al.*, *Nat. Comm.*, 2013, **4**, 1732.
13 P. Banerjee, *et al.*, *Nat. Nanotechnol.*, 2009, **4**, 292.
14 M. M. Shaijumon, *et al.*, *Adv. Mater.*, 2010, **22**, 4978.
15 N.-S. Choi, *et al.*, *J. Mater. Chem.*, 2011, **21**, 9825.
16 L. Taberna, *et al.*, *Nat. Mater.*, 2006, **5**, 567.
17 S. K. Cheah, *et al.*, *Nano Lett.*, 2009, **9**, 3230.
18 A. Vlad, *et al.*, *Proc. Natl. Acad. Sci. U. S. A.*, 2012, **109**, 15168.
19 G. Sandu, *et al.*, *ACS Nano*, 2014, **8**, 9427.
20 S. Xiong, *et al.*, *CrystEngComm*, 2011, **13**, 626.
21 C. Wei, *et al.*, *Sci. Rep.*, 2013, 3.

22 D. Wang, *et al.*, *Chem. Mater.*, 2006, **18**, 4231.
23 J. Martín, *et al.*, *Nat. Commun.*, 2014, **5**, 5130.
24 C.-C. Lo, *et al.*, *J. Magn. Magn. Mater.*, 2011, **323**, 1950.
25 C.-M. Liu, *et al.*, *J. Electrochem. Soc.*, 2012, **159**, K78.
26 S. J. Dillon and K. Sun, *Curr. Opin. Solid State Mater. Sci.*, 2012, **16**, 153.
27 J. F. M. Oudenhoven, *et al.*, *Adv. Energy Mater.*, 2010, **1**, 10.
28 A. Vlad, *et al.*, *Small*, 2008, **4**, 557.